305

no

MSC INTERNAL NOTE NO. 65-EG-42

PROJECT APOLLO

A LINEAR, SINGLE-PLANE STUDY OF THE EFFECT OF SPS ACTUATOR COMPLIANCE ON THE RESPONSE CHARACTERISTICS OF THE APOLLO BLOCK I SCS

Prepared by: _____
Emery E. Smith, Jr.

Approved: _____
David W. Gilbert, Chief, Engineering Simulation Branch

Approved: _____
Robert G. Chilton, Deputy Chief, Guidance and Control Division

NATIONAL AERONAUTICS AND SPACE ADMINISTRATION

MANNED SPACECRAFT CENTER

Houston, Texas

September 23, 1965

FACILITY FORM 602

N70-75883 (ACCESSION NUMBER) (THRU)

32 (PAGES) NONE (CODE)

TMX-65192 (NASA CR OR TMX OR AD NUMBER) (CATEGORY)

SUMMARY

A linear, single-plane (yaw-axis) study of the Apollo Block I SPS actuator compliance effects on the SPS actuator servo itself and on the overall SCS has been made by the Guidance and Control Division. The SCS configuration and vehicle and actuator dynamics are those defined in the reference. The data obtained from these analyses indicate that although the compliance effects can be seen in the system response, they are not detrimental to operations.

INTRODUCTION

A determination of autopilot system stability including the effects of actuator compliance cross-coupling requires a three-axis study. However, due to the complexity of the problem, no mathematical model has been developed at present. This study has gone into the analysis of the small amplitude, linear, single-plane model of the compliance which can be incorporated in future Apollo control system simulations when applicable.

The immediate objectives of the study were to: (1) determine the transfer function and frequency response characteristics of the SPS with and without compliance using the math model of the reference, and (2) determine the stability gain and phase margin of the SCS with SPS compliance included.

SYSTEM DESCRIPTION

A block diagram of the SPS without compliance is shown in figure 1 and figure 4 is the complete autopilot system, including the SPS actuator compliance math model analyzed in this study. Figure 2 shows the simplified diagram of the yaw actuator from which the compliance math model was derived, and figure 3 is the general CSM configuration with the primary parameters of interest in this study. Note that a change in actuator length causes the engine and gimbal assembly to rotate about the body mount bearing. Also, the snubber stiffness shown in figure 2 is not accounted for in the equations since its effect is only seen when the actuator is at the limit of its travel.

RESULTS

An analysis of the frequency response of the rate and position loops of the SPS without actuator compliance indicates a phase margin of about 70 degrees and a gain margin of about 32 db for the rate loop and a phase margin of about 60 degrees and a gain margin of about 12.5 db for the position loop. Frequency responses of the open and closed loops of the SPS are contained in figures 5 through 8.

Analysis of the SPS with actuator compliance included was started by reducing the gimbal-actuator system equations 2, 3, 4, and 5 (omitting DWT effects) to transfer function form using flow graph reduction techniques (figure 9). The final result of the reduction, which provided the transfer functions δ_T/T' and δ_{po}/δ_T in both symbolic and numerical form (using parameter values from the reference), is shown in figure 10. The overall block diagram of the compliant SPS actuator servo and its closed-loop transfer function (containing numerical values determined from the parameters of the reference) are contained in figure 11. Open and closed loop frequency responses of the rate and position loops of the SPS were determined using the data of this figure.

The open loop frequency response (figure 12) and Nyquist plot (figure 13) of the rate loop indicate the loop to have a phase margin of about 70 degrees and a gain margin of about 20 db. The closed loop response of the rate loop is shown in the Bode plot of figure 14. Figure 15 and 16, the open loop frequency response and Nyquist plot of the SPS position loop, respectively, show the loop to have a phase margin of about 60 degrees and a gain margin of 12.5 db. The frequency plot of figure 17 represents the closed loop position response.

Adding the vehicle attitude and attitude rate loops to the SPS (figure 18) and substituting parameters for the CSM with one quarter fuel loading yields the SCS block diagram of figure 19. Open and closed loop frequency responses of the SCS (autopilot) rate and position loops are shown in figures 20 to 23. The open loop responses of the rate loop (figure 20) indicates the phase margin to be about 80 degrees and the gain margin of about 17 db. The open loop responses of the position loop (figure 22) shows a phase margin of about 55 degrees and a gain margin of about 14 db.

It should be noted that 360 degrees is the initial zero point on the phase plots of the frequency response. To make these plots, the logic of the computer notes only four quadrants and there are no negative angles. To find phase lag, subtract the plot reading from 360 degrees making note of the number of cycles the response has already been through.

CONCLUDING REMARKS

The frequency response characteristics of the SPS and SCS determined using the model defined herein show this linear, single-plane system to be stable in the presence of SPS actuator compliance and to possess adequate gain and phase margins. Future studies of the actuator compliance effects are planned and will be specified in forthcoming presimulation reports. The studies will investigate (1) the effect of actuator compliance on the autopilot in the presence of system nonlinearities, body bending, and propellant slosh; (2) the effect of actuator mount stiffness on the autopilot; and (3) the effect of actuator compliance on Apollo Block I SCS small signal stability.

SYMBOL DEFINITION

D_e	- Distance from engine gimbal to engine c.m. along the engine center line; ft
D_x	- Distance from engine gimbal to system c.m. along the body x-axis; ft
F	- Engine thrust; lbs
I_{zz}	- Moment of inertia of system about c.m.; lb-ft-sec^2
J_a	- Moment of inertia of bull gear and clutch reflected to bull gear; lb-ft-sec^2
J_n	- Nozzle moment of inertia about engine c.m.; lb-ft-sec^2
K_a	- Actuator arm stiffness; lb/ft
K_c	- Forward loop gain constant; N.D.
K_L	- Gimbal stiffness; lb/ft
K_T	- Actuator mount stiffness; lb/ft
K_i	- Actuator servo amplifier gain; amp/rad
K_η	- Clutch gain; ft-lb/amp
$K_{\dot{\delta}}$	- Actuation system rate feedback gain constant; rad/rad/sec
K_δ	- Actuation system nozzle position feedback gain constant; N.D.
$K_{\dot{\psi}}$	- SCS rate gyro feedback gain constant; rad/rad/sec
K_ψ	- SCS attitude gain constant; N.D.
M_E	- Engine mass; slugs
N	- Pitch of screw jack; rad/ft
N^2B_θ	- Total damping of actuator lumped at tachometer, reflected to engine; lb-sec/ft
R	- Actuator lever arm; ft
S	- LaPlacian operator; "sec^{-1}"

SYMBOL DEFINITION (Continued)

T	- Clutch torque; ft-lb
X_2	- Actuator mount deflection; ft
δ	- Gimbal position; rad
δ_c	- Gimbal position command; rad
δ_{po}	- Pickoff position; radians of gimbal deflection
δ_T	- Tachometer position; rad
ψ	- Attitude position; rad
T'	- $T/R^2N^2J_a$

In addition, a dot over a symbol represents a time rate of change of that variable

REFERENCE

1. NAA Internal Letter 697-521-110-64-1060 dated November 9, 1964, "Nonlinear Study of the Block I Autopilot"

TABLE I

Constants

Quantity	Value	Units
D_e	.667	Ft.
D_x	9.62	Ft.
F	21900.	Lbs.
I_{zz}	52400.	Ft-lb-sec^2
J_a	$70/(96\pi)^2$	Ft-lb-sec^2
J_n	220	Ft-lb-sec^2
K_a	1.2×10^6	Lb/ft
K_c	1.5	N.D.
K_L	2.0×10^6	Lb/ft
K_T	$.576 \times 10^6$	Lb/ft
K_ϵ	20	amps/rad
K_η	3530	Ft-lb/amp
$K_{\dot{\delta}}$	.09	rad/rad/sec
K_δ	1.0	N.D.
$K_{\dot{\psi}}$	.5	rad/rad/sec
K_ψ	1.0	N.D.
M_E	20	Slugs
N	96π	rad/ft
N^2B_θ	2000	lb-sec/ft
R	1.	Ft.

LIST OF FIGURES

Figure	Title
1	Service Propulsion Actuation System
2	Actuator
3.	CSM Configuration
4	Autopilot
5	Frequency response, SPS rate loop open, w/o compliance (δ_R/ϵ)
6	Frequency response, SPS rate loop closed, w/o compliance (δ_R/δ_ϵ)
7	Frequency response, SPS position loop open, w/o compliance (δ_F/δ_ϵ)
8	Frequency response, SPS position loop closed, w/o compliance (δ_R/δ_ϵ)
9	Gimbal-actuator dynamics
10	($\dot{\delta}_T/T^1$); ($\delta_{po}/\dot{\delta}_T$)
11	Service Propulsion Actuation System
12	Frequency response, SPS rate loop open (δ_R/ϵ)
13	Frequency response, SPS rate loop open, Nyquist plot (δ_R/ϵ)
14	Frequency response, SPS rate loop closed (δ_R/δ_ϵ)
15	Frequency response, SPS position loop open (δ_F/δ_ϵ)
16	Frequency response, SPS position loop open, Nyquist plot (δ_F/δ_ϵ)
17	Frequency response, SPS position loop closed (δ_F/δ_ϵ)

LIST OF FIGURES (Continued)

Figure	Title
18	Vehicle Dynamics
19	Stabilization & Control System
20	Frequency response, attitude rate loop open (ψ_R/δ_c)
21	Frequency response, attitude rate loop closed (ψ_R/ψ_ϵ)
22	Frequency response, attitude position loop open (ψ_F/ψ_ϵ)
23	Frequency response, attitude position loop closed (ψ_F/ψ_c)

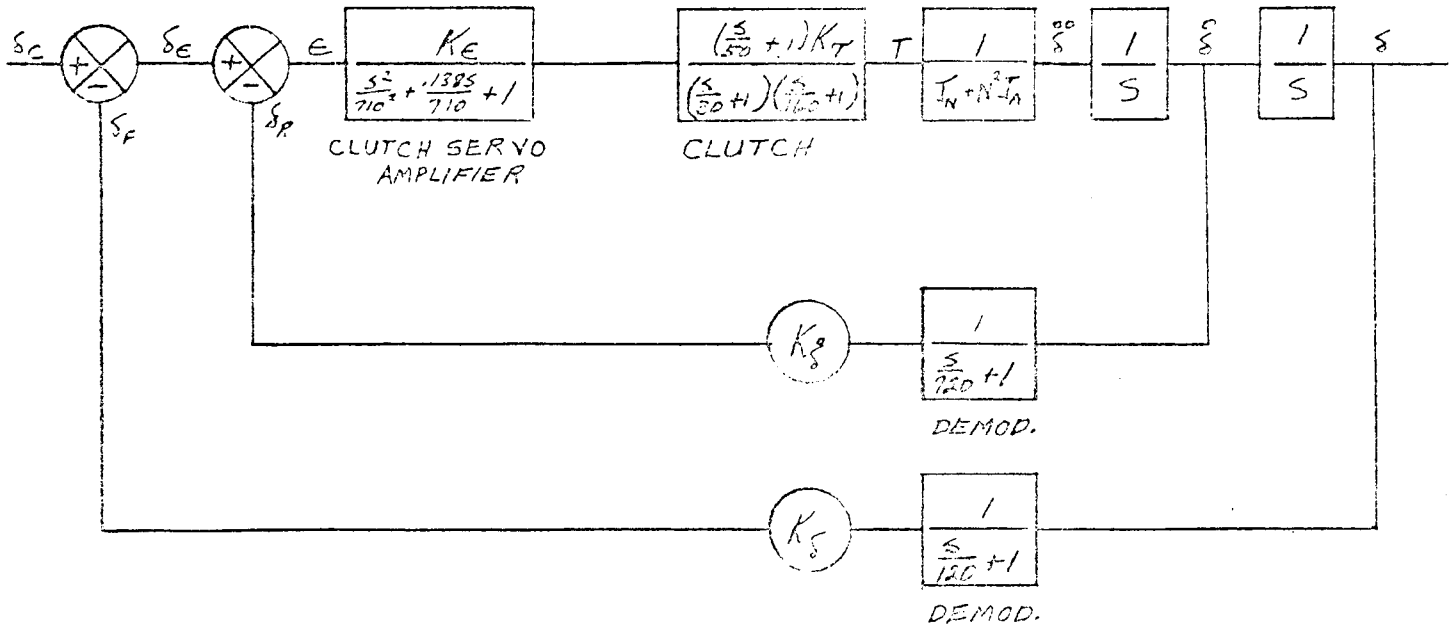

SERVICE PROPULSION ACTUATION SYSTEM

FIGURE 1

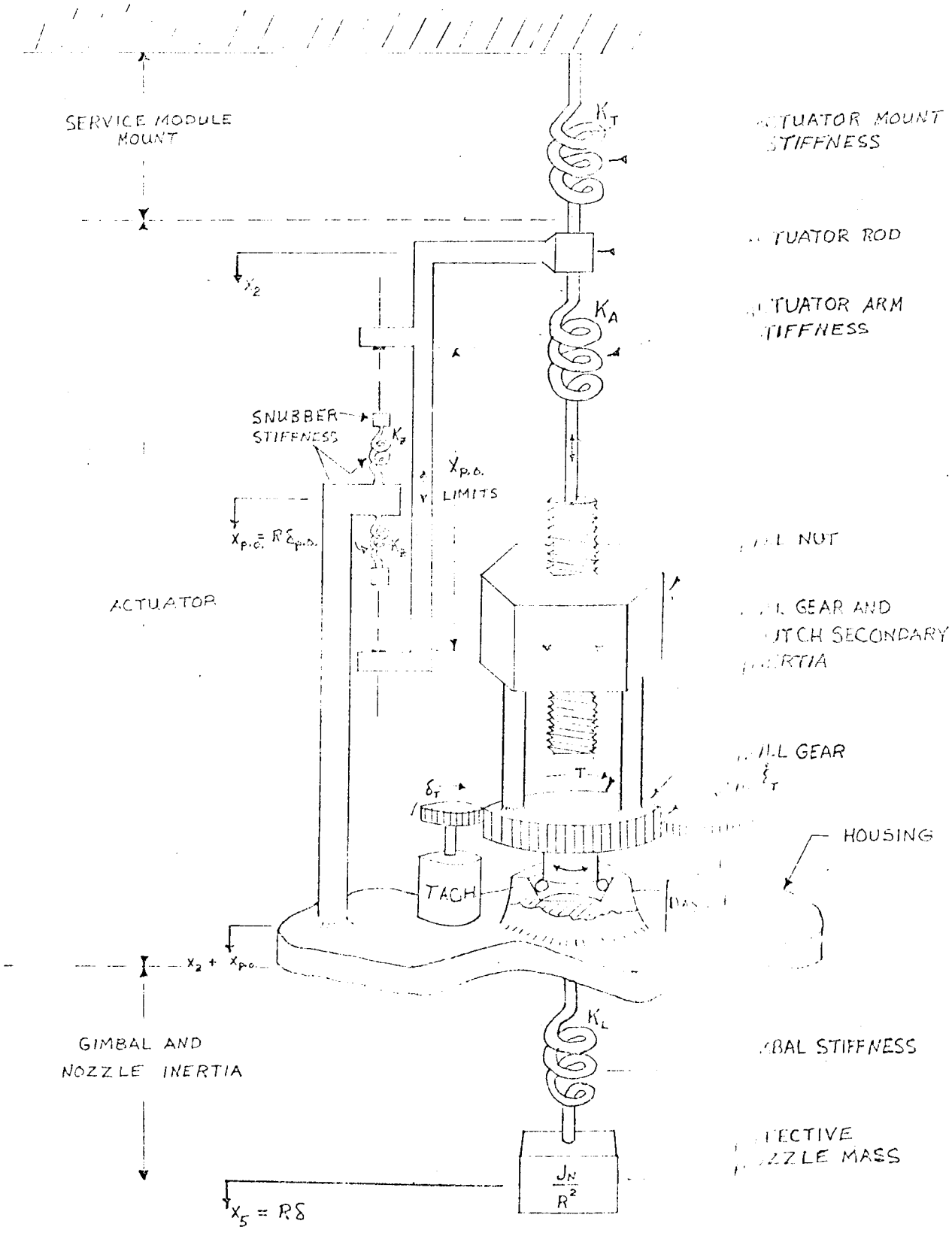

ACTUATOR

FIGURE 2

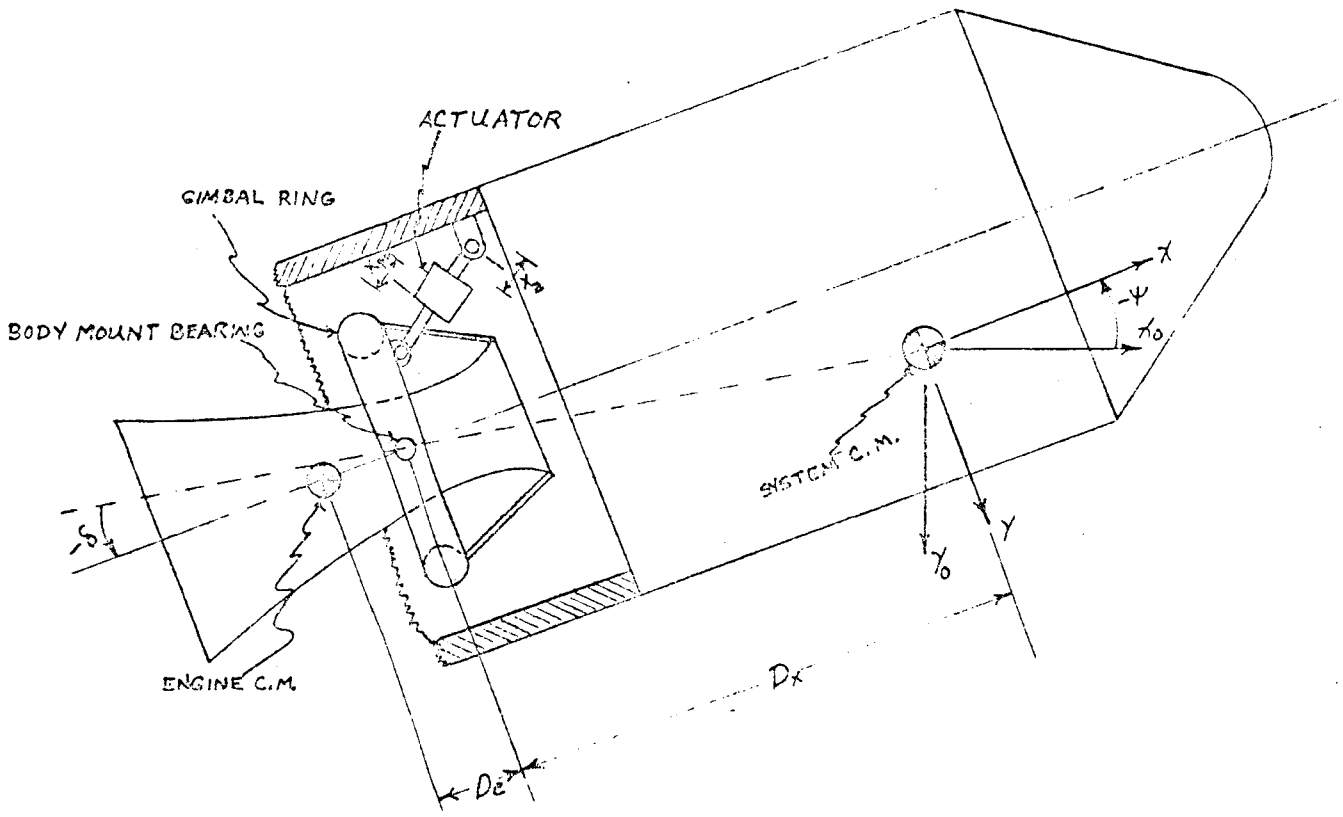

CSM CONFIGURATION

FIGURE 3

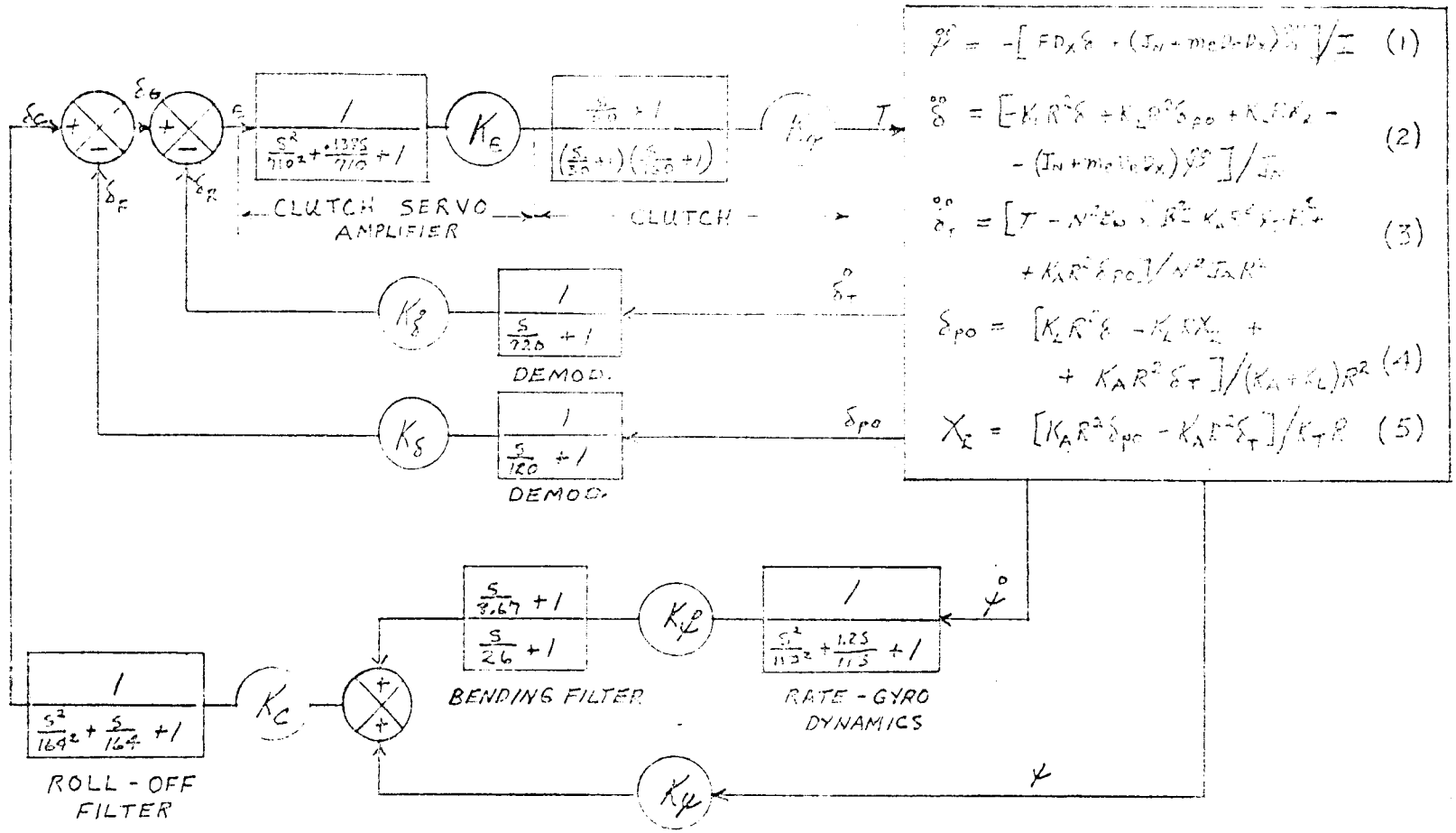

AUTOPILOT

FIGURE 4

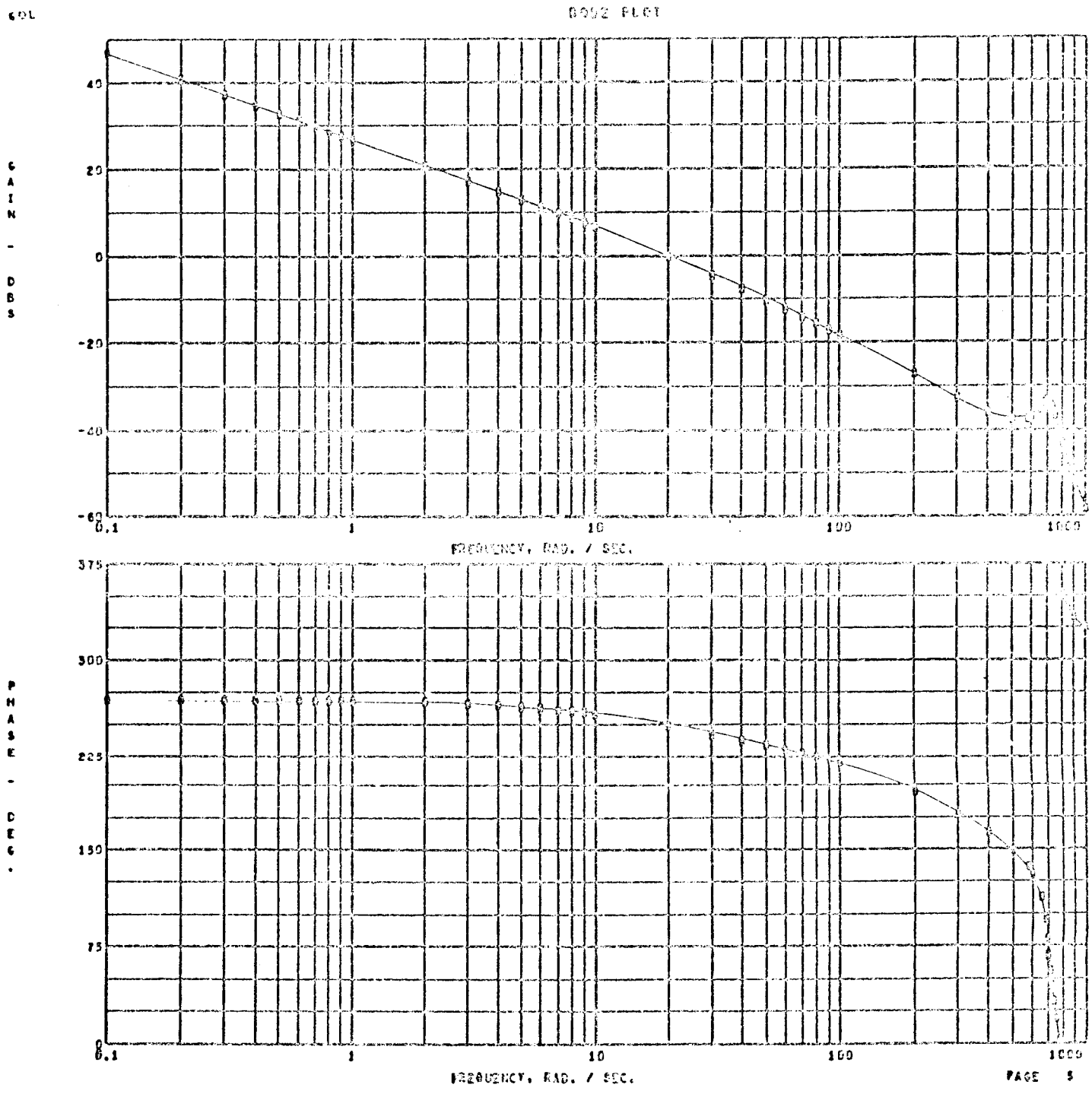

Frequency Response
SPS Rate Loop Open
W/O Compliance
(δ_R/ϵ)

Figure 5

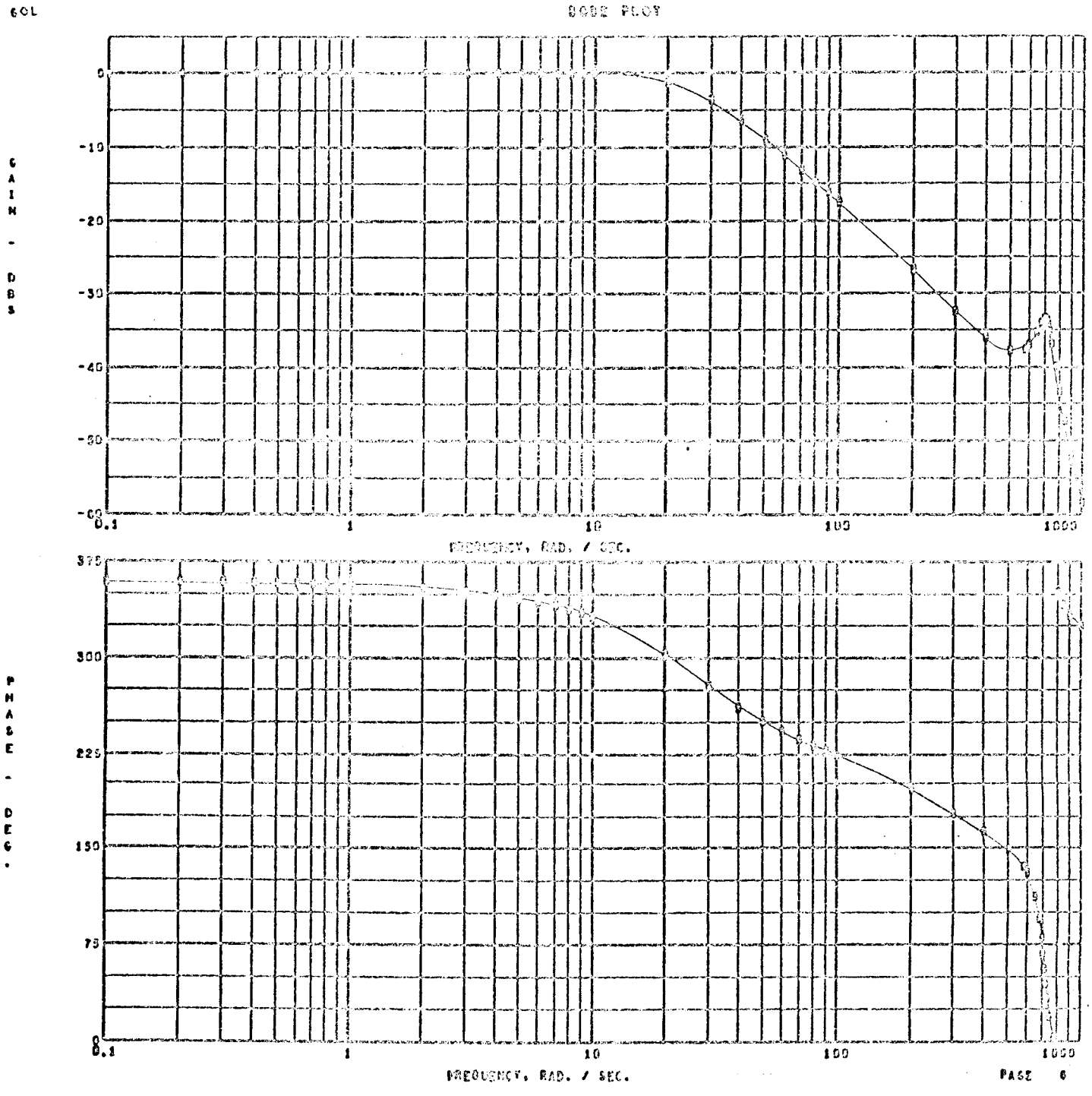

Frequency Response
SPS Rate Loop Closed
W/O Compliance
(δ_p/δ_c)
Figure 6

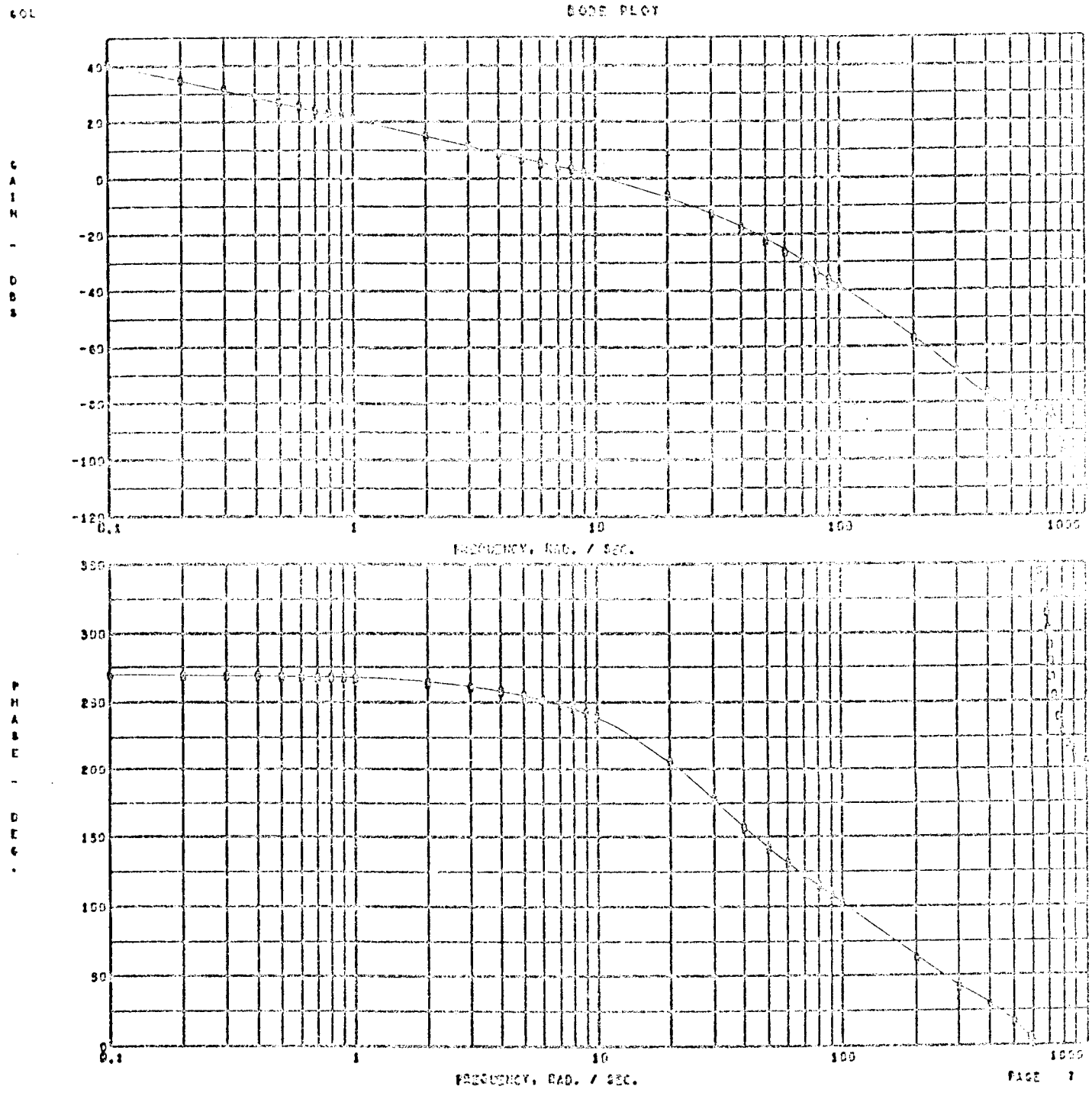

Frequency Response
SPS Position Loop Open
W/O Compliance
(δ_p/δ_e)

Figure 7

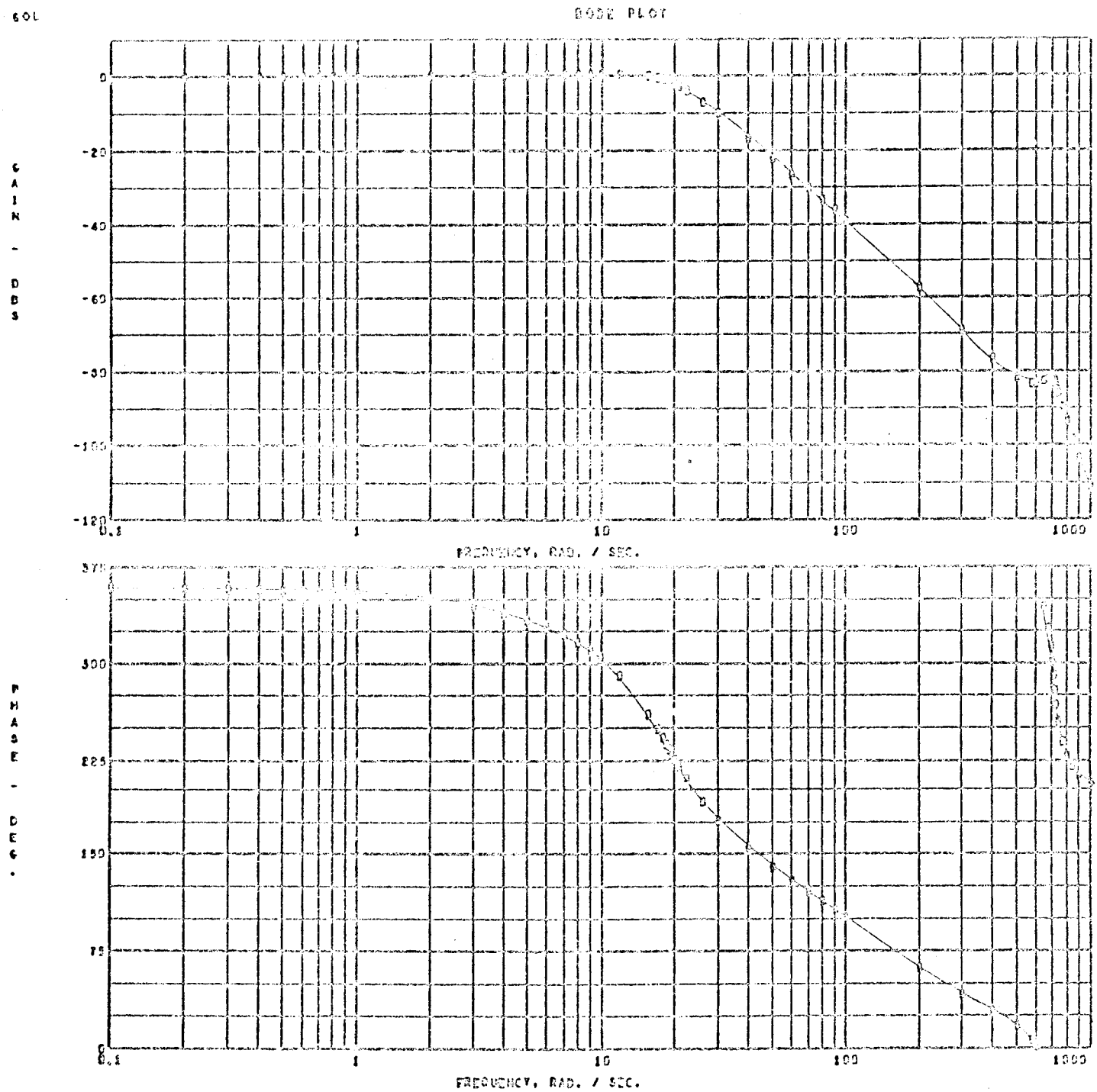

Frequency Response
SPS Position Loop Closed
W/O Compliance
(δ_F/δ_c)

Figure 8

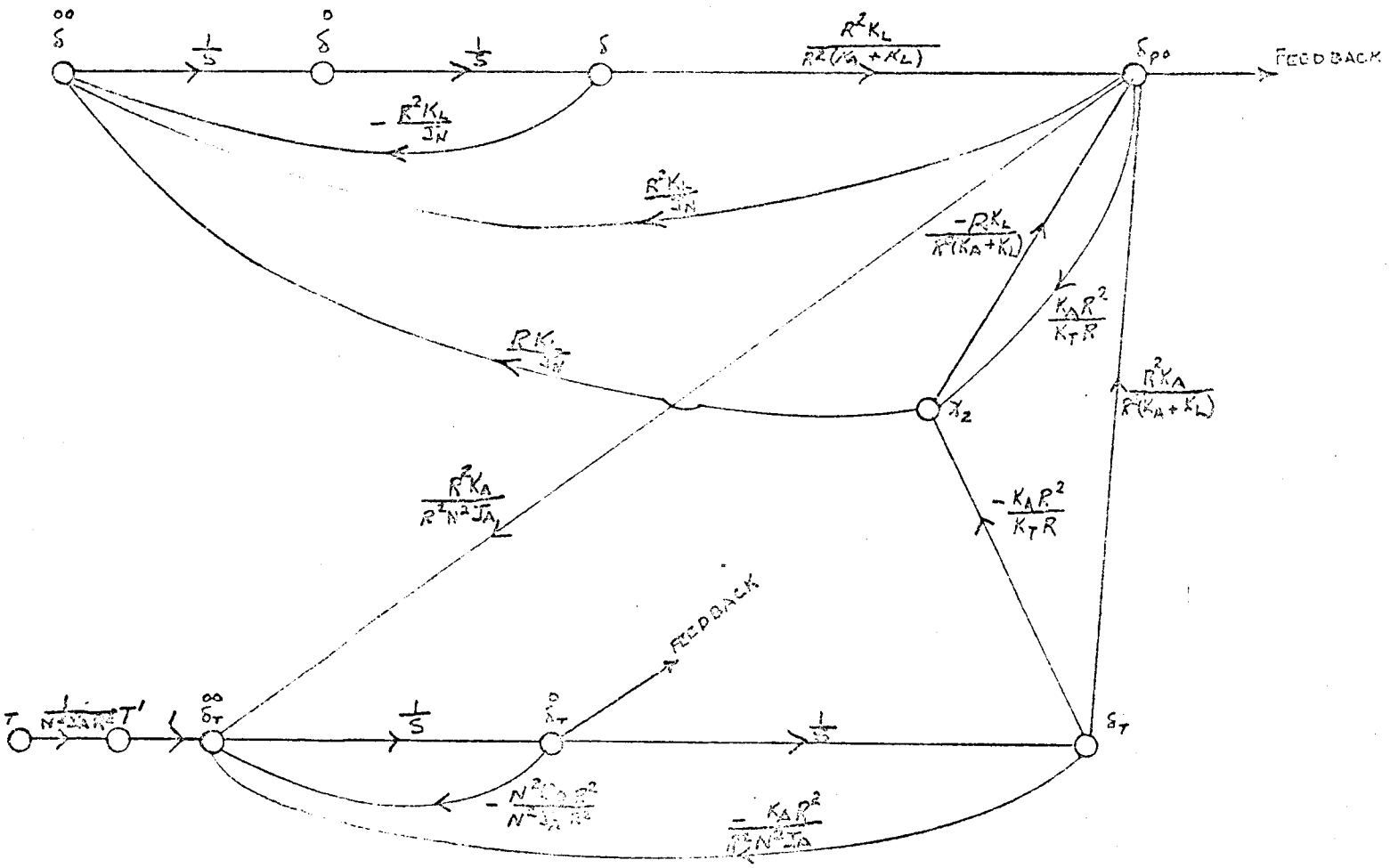

GIMBAL-ACTUATOR DYNAMICS

FIGURE 9

(a)

$$T' \;\Bigg|\; \frac{S\left[\left(S^2+\frac{K_L R^2}{J_N}\right)-\frac{K_L R^2}{J_N}\left(1+\frac{K_A}{K_T}\right)\left(\frac{K_L K_T}{K_T(K_A+K_L)+K_A K_L}\right)\right]}{\left(S^2+\frac{N^2 B_{eq}}{N^2 J_A}S+\frac{K_A}{N^2 J_A}\right)\left[\left(S^2+\frac{K_L R^2}{J_N}\right)-\left(\frac{K_L R^2}{J_N}\right)\left(1+\frac{K_A}{K_T}\right)\left(\frac{K_T K_L}{K_T(K_A+K_L)+K_A K_L}\right)\right]-\frac{K_A}{N^2 J_A}\left[\frac{K_A}{K_T(K_A+K_L)+K_A K_L}\left((K_L+K_T)S^2+\frac{R^2 K_T K_L}{J_N}\right)\right]} \;\Bigg|\; \overset{\circ}{\delta}_T$$

$$T' \;\Bigg|\; \frac{.035\left(\frac{S^2}{1481}+1\right)}{\left(\frac{S^3}{42500}+\frac{S^2}{1481}+\frac{S}{6.9}+1\right)} \;\Bigg|\; \overset{\circ}{\delta}_T$$

(b)

$$\overset{\circ}{\delta}_T \;\Bigg|\; \frac{\frac{K_A}{K_T(K_A+K_L)+K_A K_L}\left[(K_T+K_L)S^2+\frac{K_T K_L R^2}{J_N}\right]}{S\left[\left(S^2+\frac{K_L R^2}{J_N}\right)-\left(\frac{K_L R^2}{J_N}\right)\left(1+\frac{K_A}{K_T}\right)\left(\frac{K_T K_L}{K_T(K_A+K_L)+K_A K_L}\right)\right]} \;\Bigg|\; \delta_{PO}$$

$$\overset{\circ}{\delta}_T \;\Bigg|\; \frac{\left(\frac{S^2}{2033}+1\right)}{S\left(\frac{S^2}{1481}+1\right)} \;\Bigg|\; \delta_{PO}$$

FIGURE 10

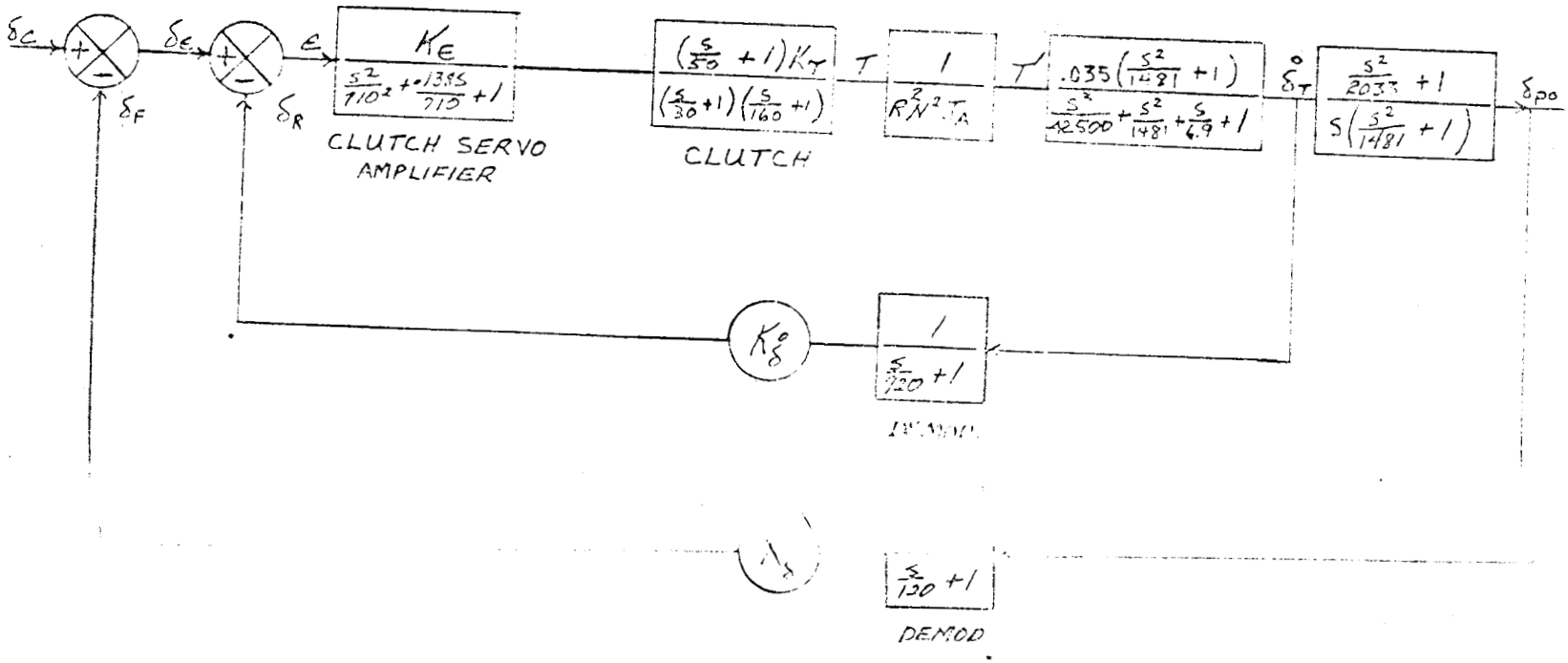

$$\delta_c \longrightarrow \boxed{\frac{\left(\frac{s}{50}+1\right)\left(\frac{s}{720}+1\right)\left(\frac{s}{120}+1\right)\left(\frac{s^2}{2033}+1\right)}{\left(\frac{s}{728}+1\right)\left(\frac{s}{14.73}+1\right)\left(\frac{s^2}{21.44^2}+\frac{2(.4932)s}{21.44}+1\right)\left(\frac{s^2}{101^2}+\frac{2(.341)s}{101}+1\right)\left(\frac{s^2}{111.5^2}+\frac{2(.986)s}{111.5}+1\right)\left(\frac{s^2}{706.8^2}+\frac{2(.074)s}{706.8}+1\right)}} \longrightarrow \delta_{po}$$

SERVICE PROPULSION ACTUATION SYSTEM

FIGURE 11

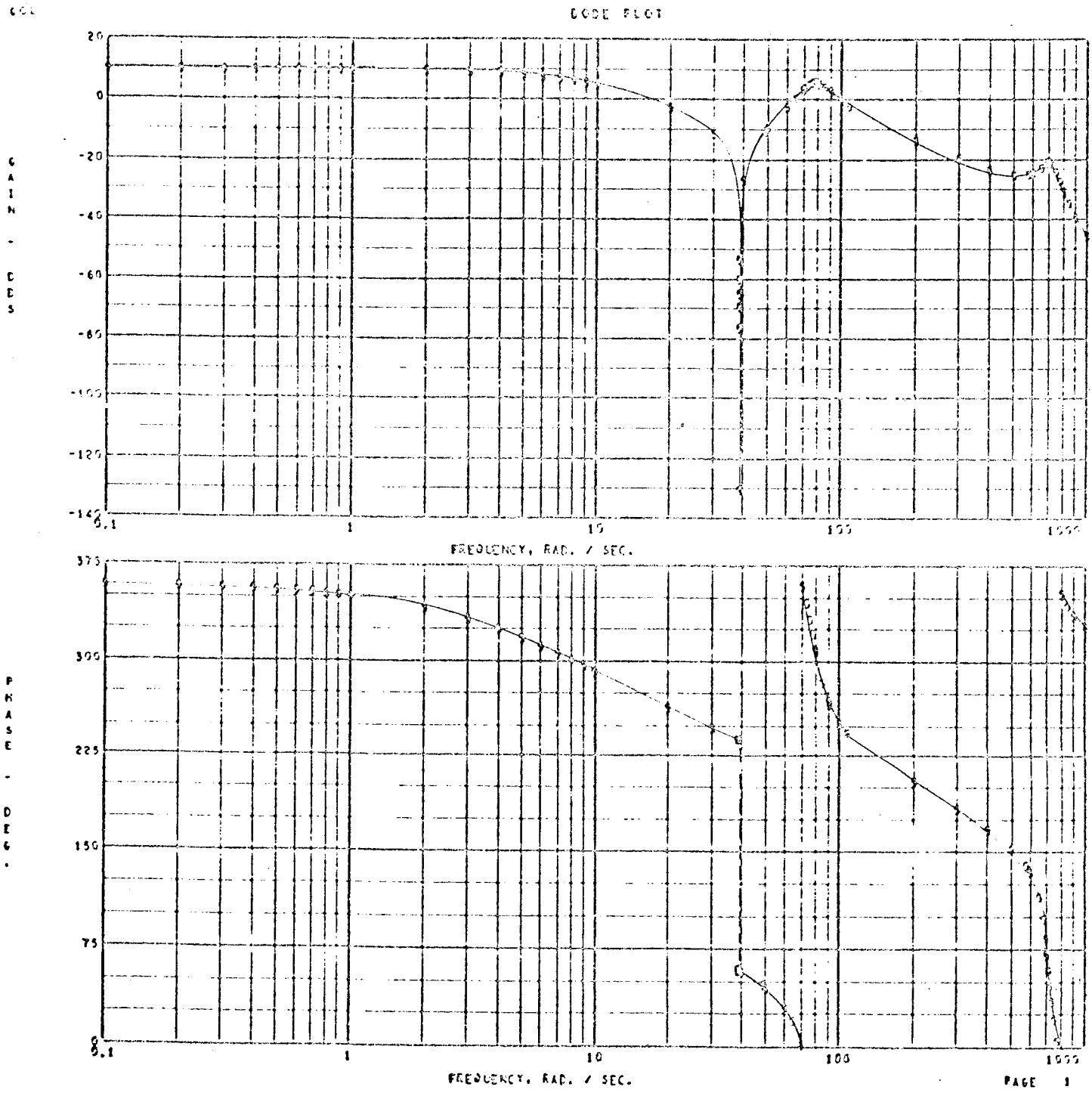

Frequency Response
SPS Rate Loop Open
(δ_R / θ)

Figure 12

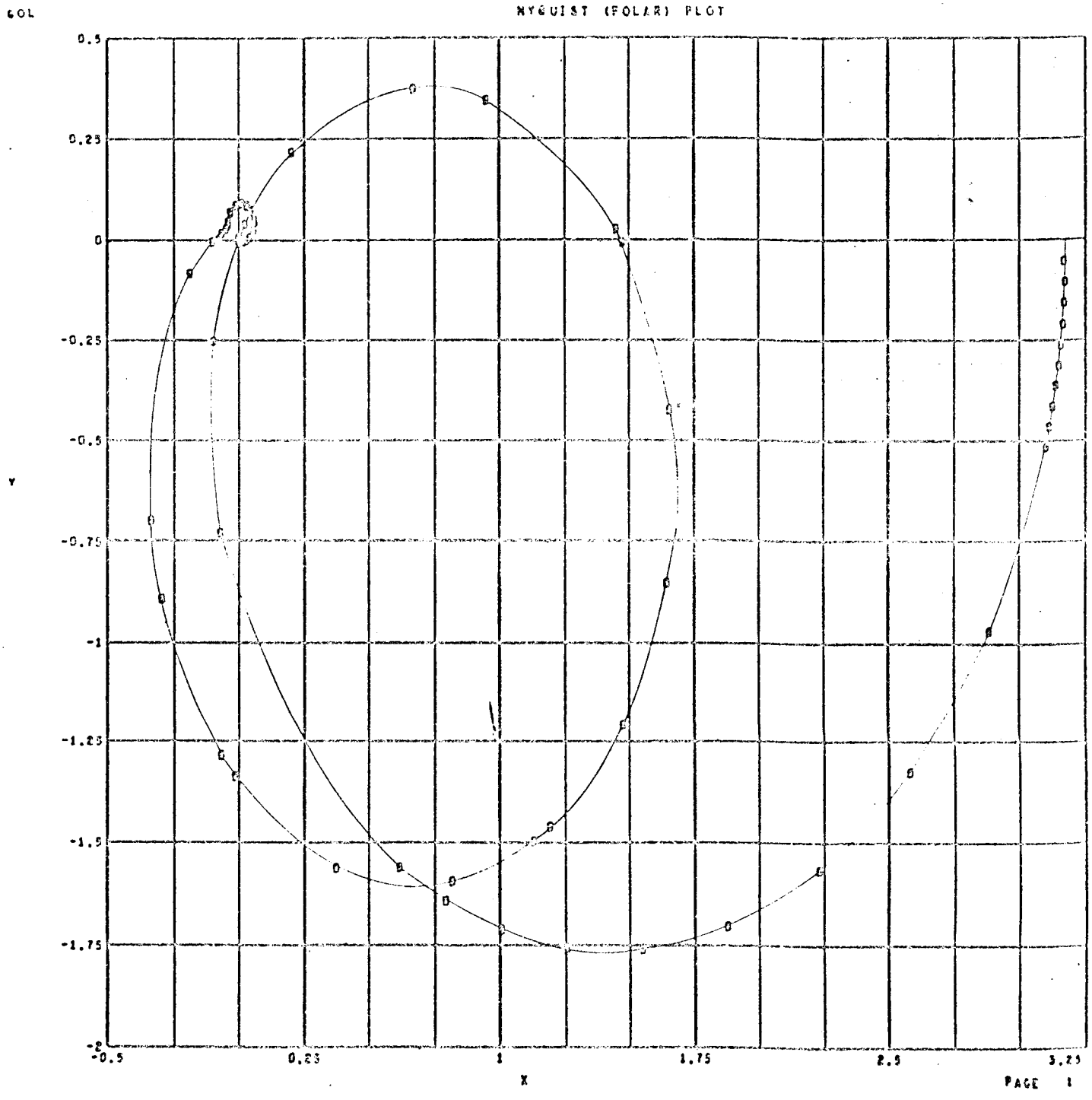

Frequency Response
SPS Rate Loop Open
(δ_R/ϵ)

Figure 13

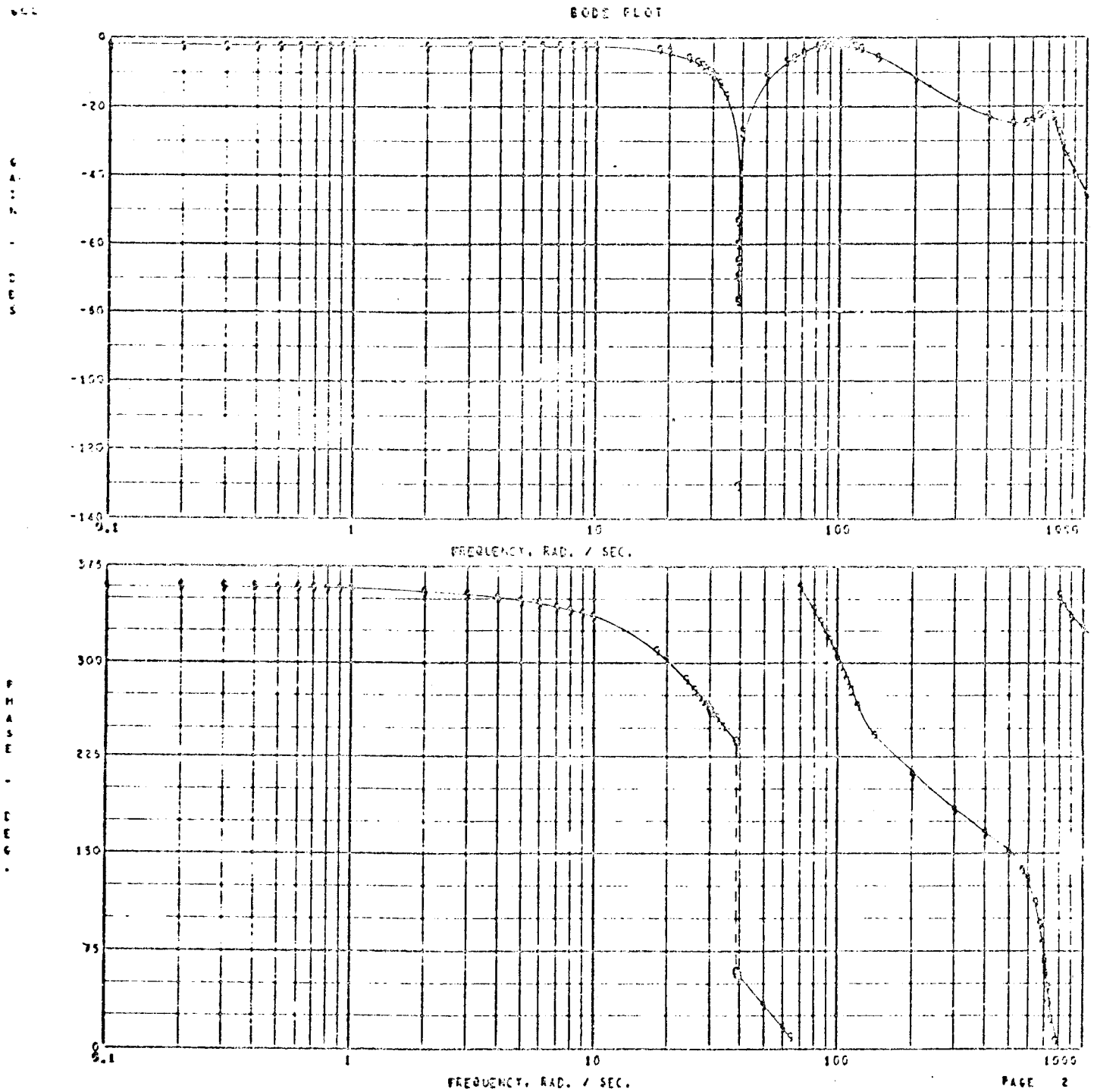

Frequency Response
SPS Rate Loop Closed
$(\delta_R / \delta_\varepsilon)$

Figure 14

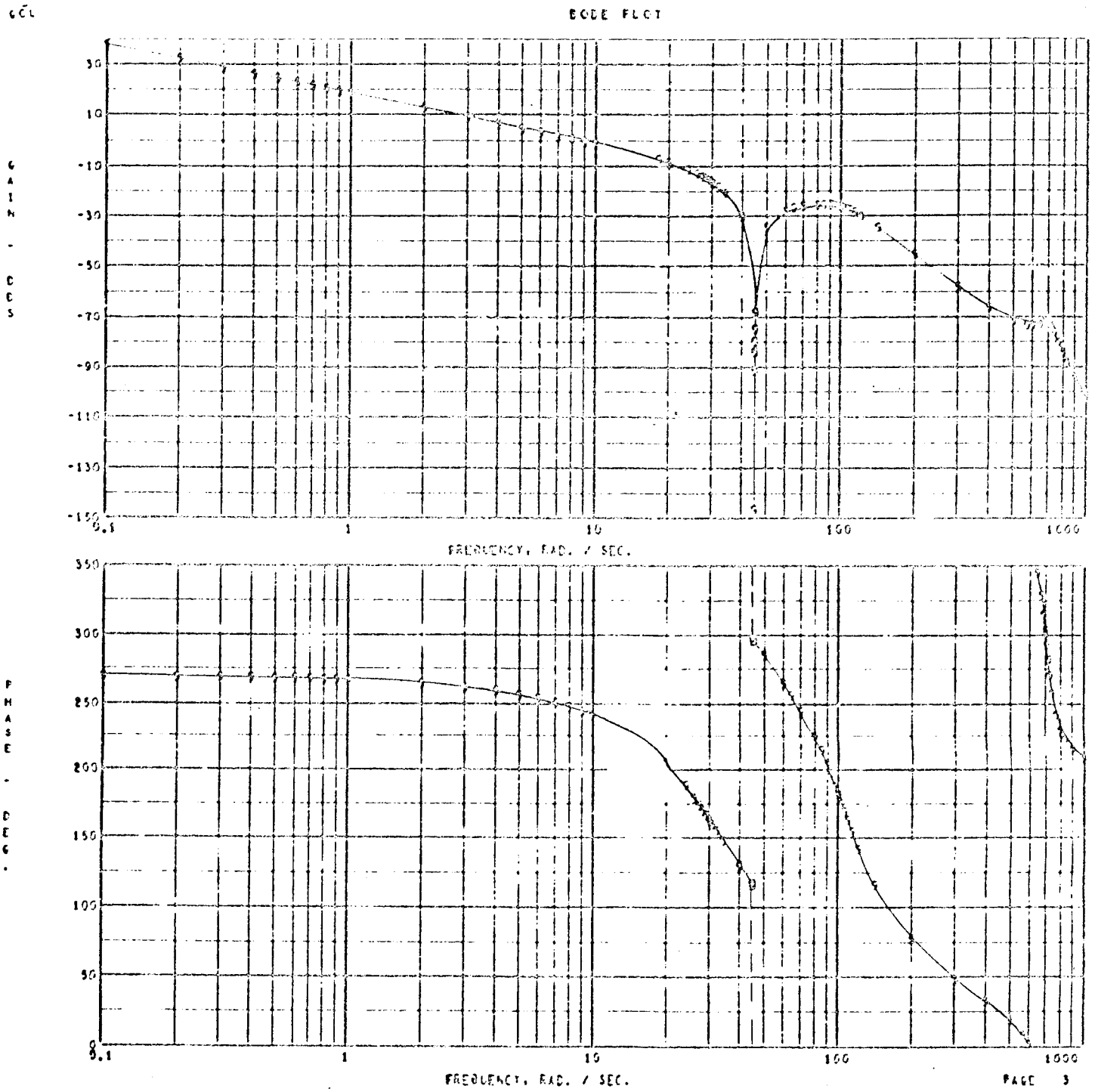

Frequency Response
SPS Position Loop Open
($\delta_F / \delta_\varepsilon$)

Figure 15

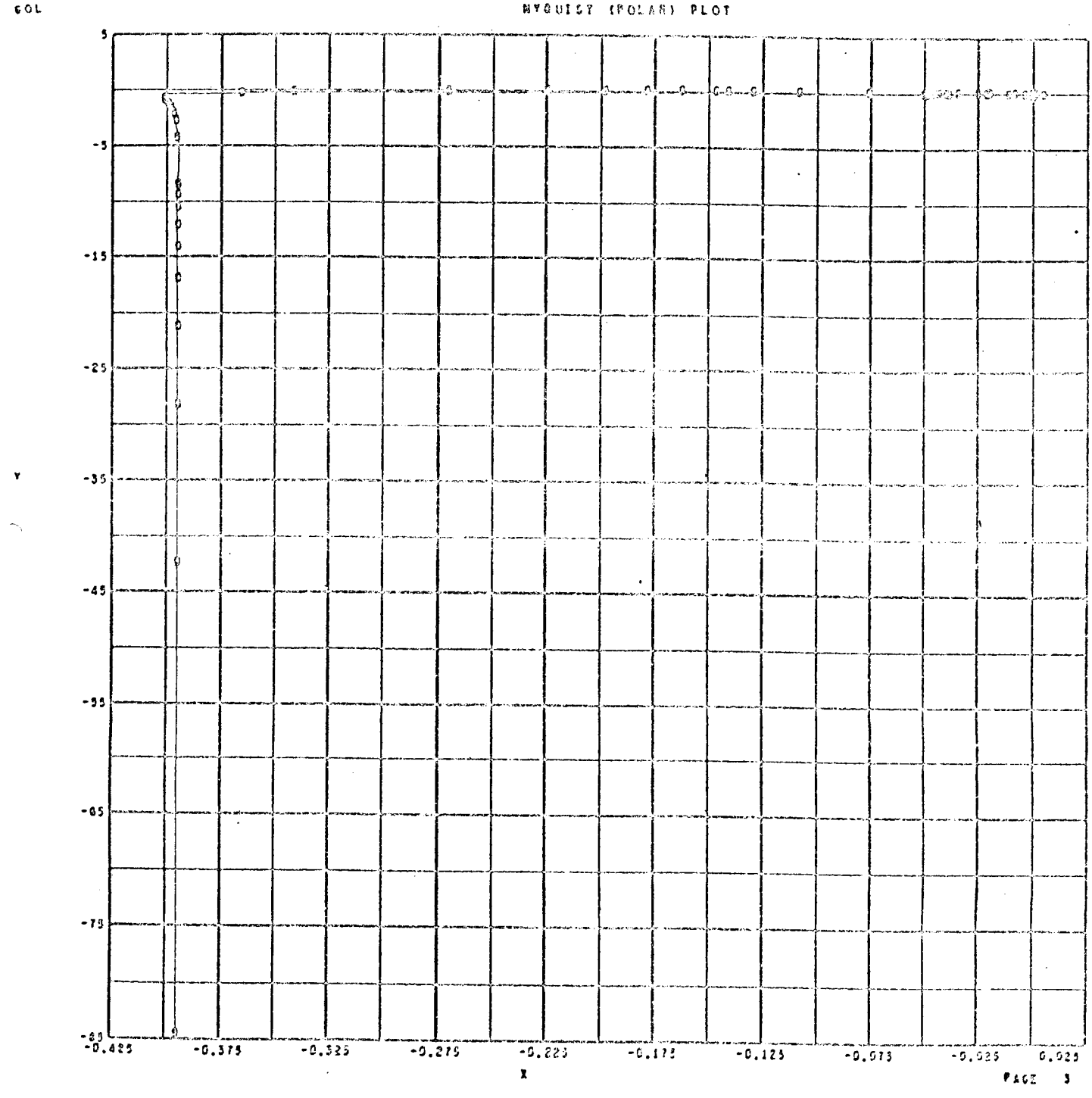

Frequency Response
SPS Position Loop Open
$(\delta_F / \delta_\epsilon)$

Figure 16

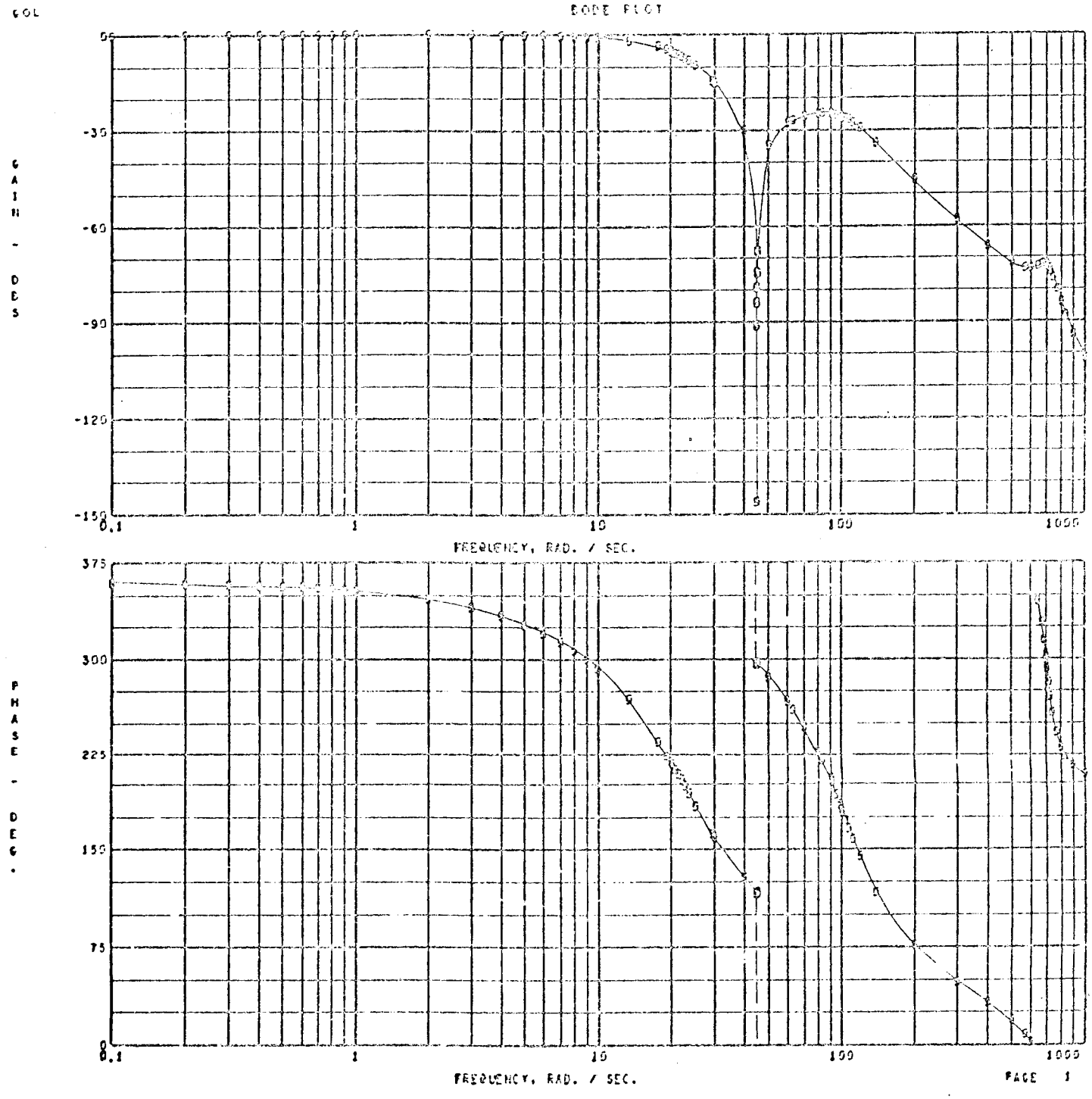

Frequency Response
SPS Position Loop Closed
(δ_F/δ_C)

Figure 17

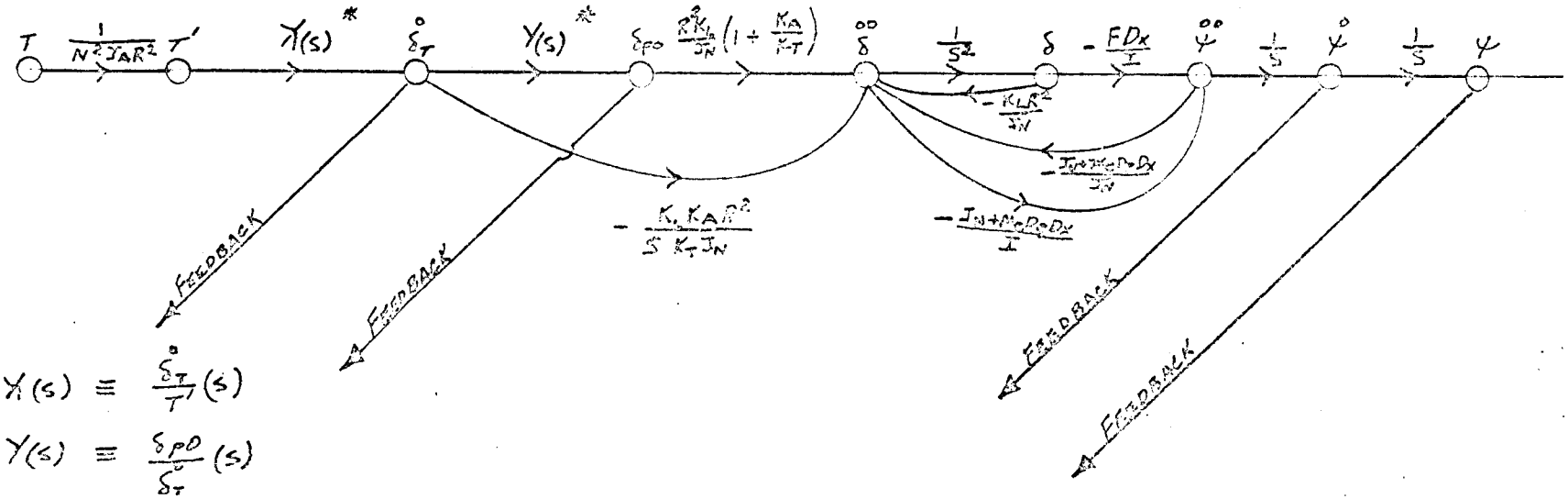

$$* \; Y(s) \equiv \frac{\delta_T^{\circ}}{T}(s)$$

$$* \; Y(s) \equiv \frac{\delta_{PO}}{\delta_T^{\circ}}(s)$$

VEHICLE DYNAMICS

FIGURE 18

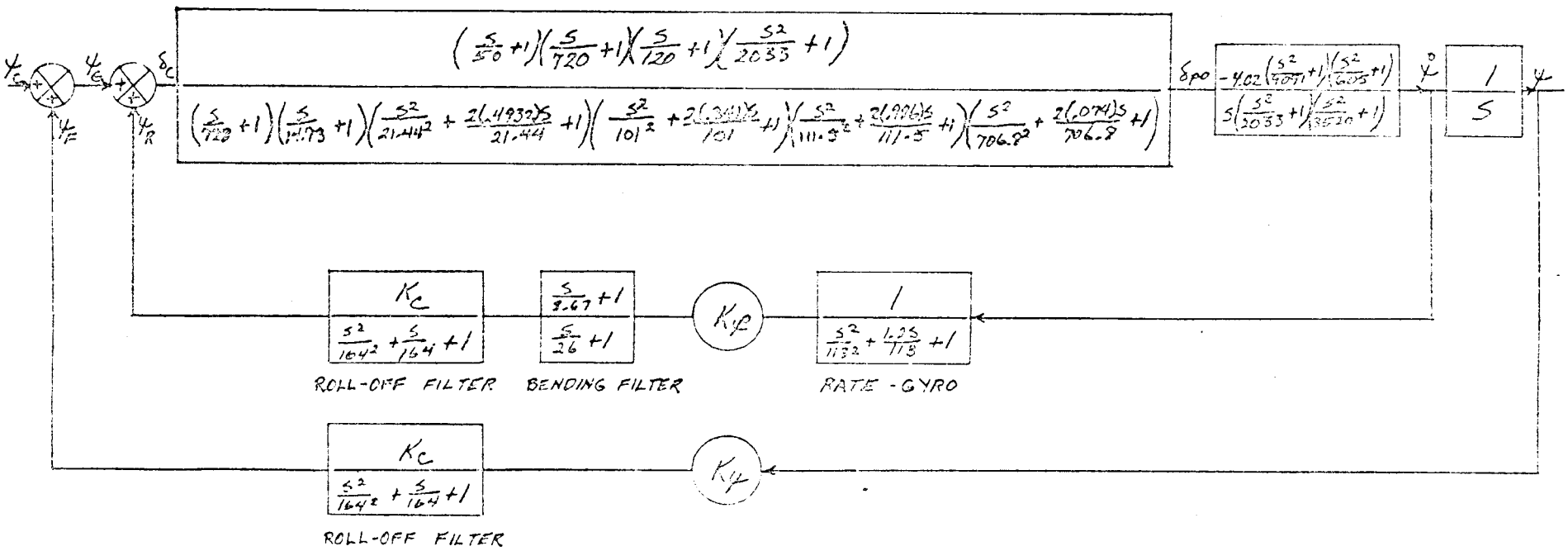

STABLIZATION & CONTROL SYSTEM

FIGURE 19

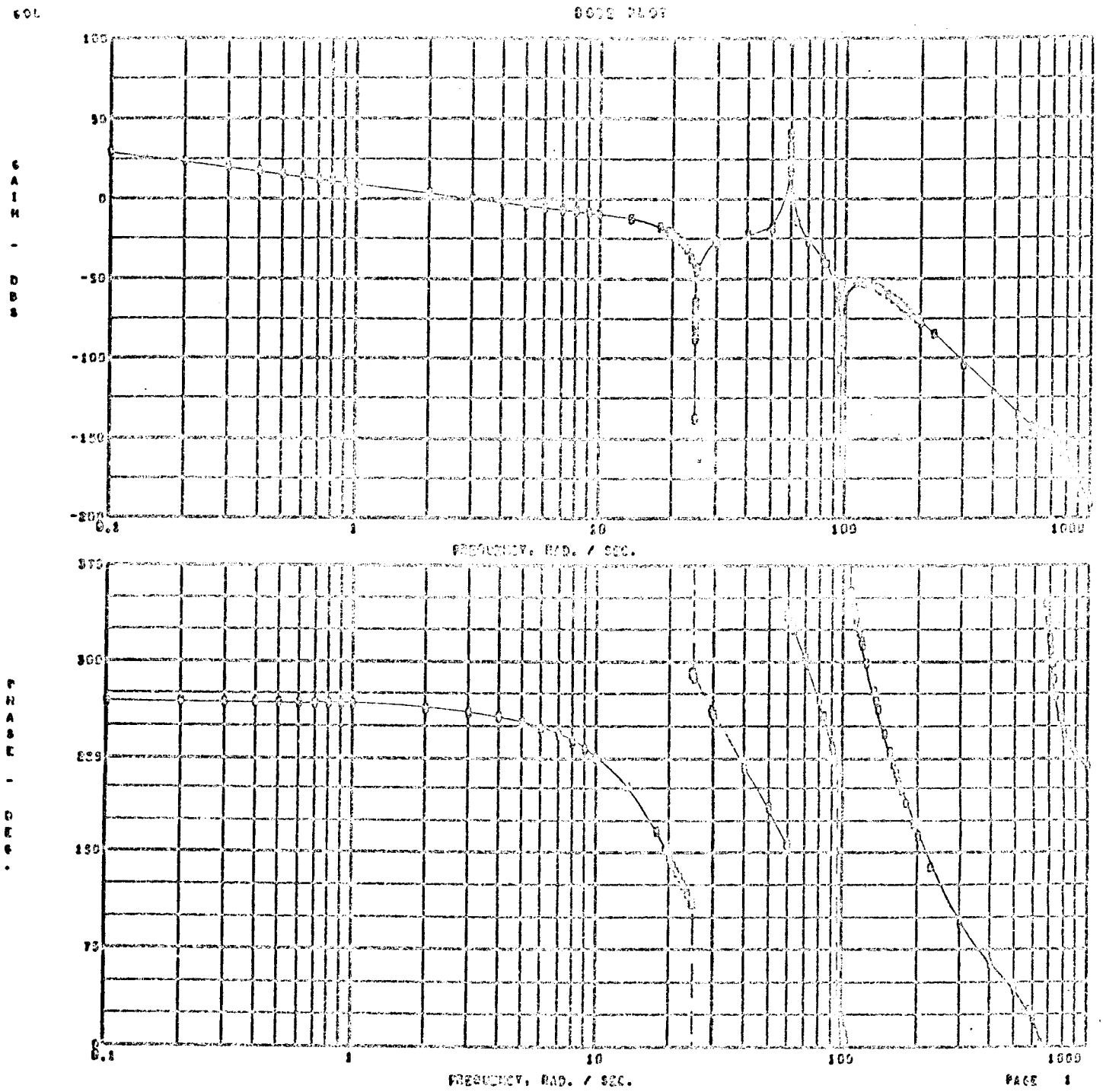

Frequency Response
Attitude Rate Loop Open
(γ_R/δ_C)

Figure 20

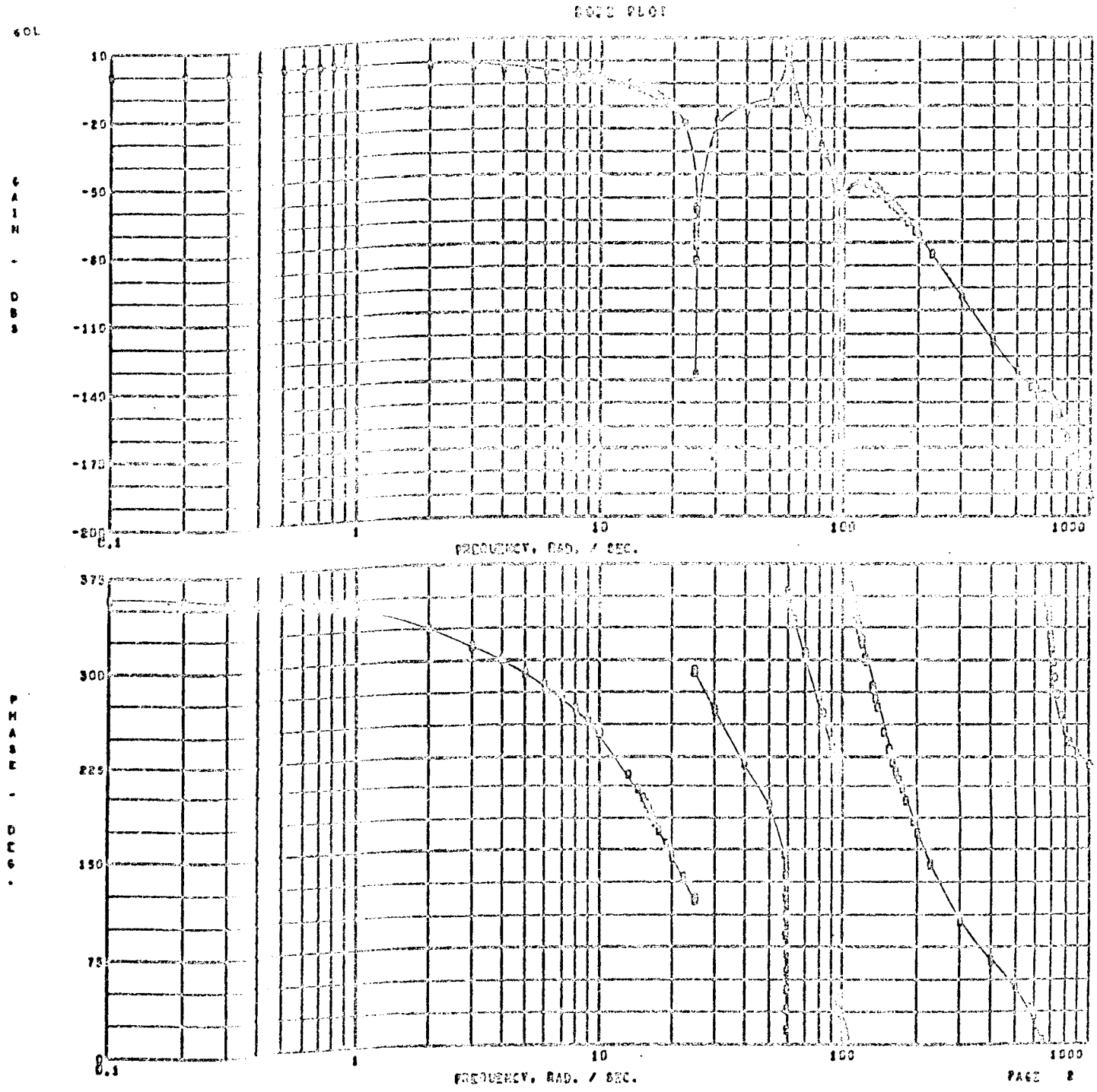

Frequency Response
Attitude Rate Loop Closed
(ψ_R / ψ_G)

Figure 21

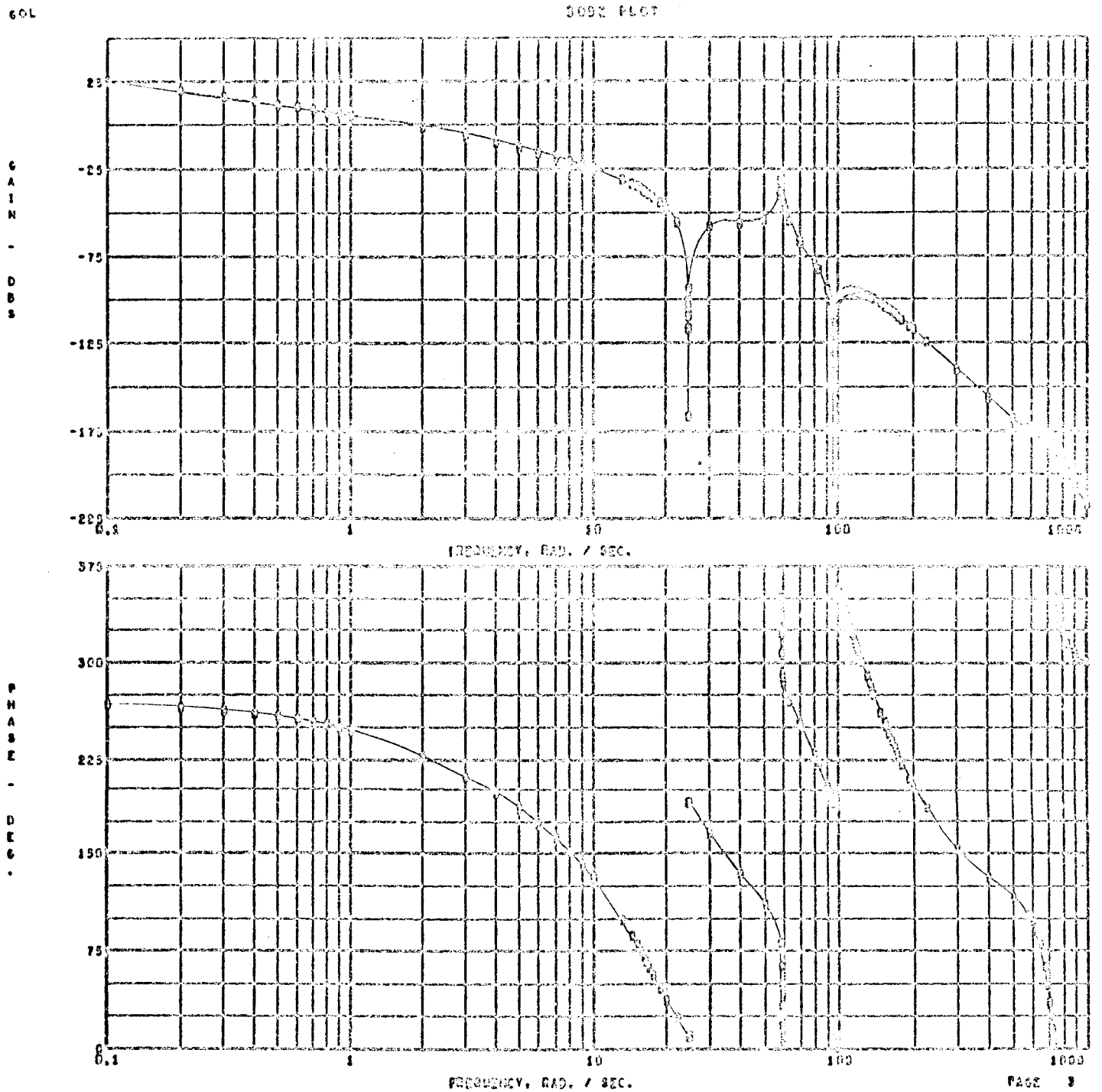

Frequency Response
Attitude Loop Open
(ψ_F / δ_E)

Figure 22

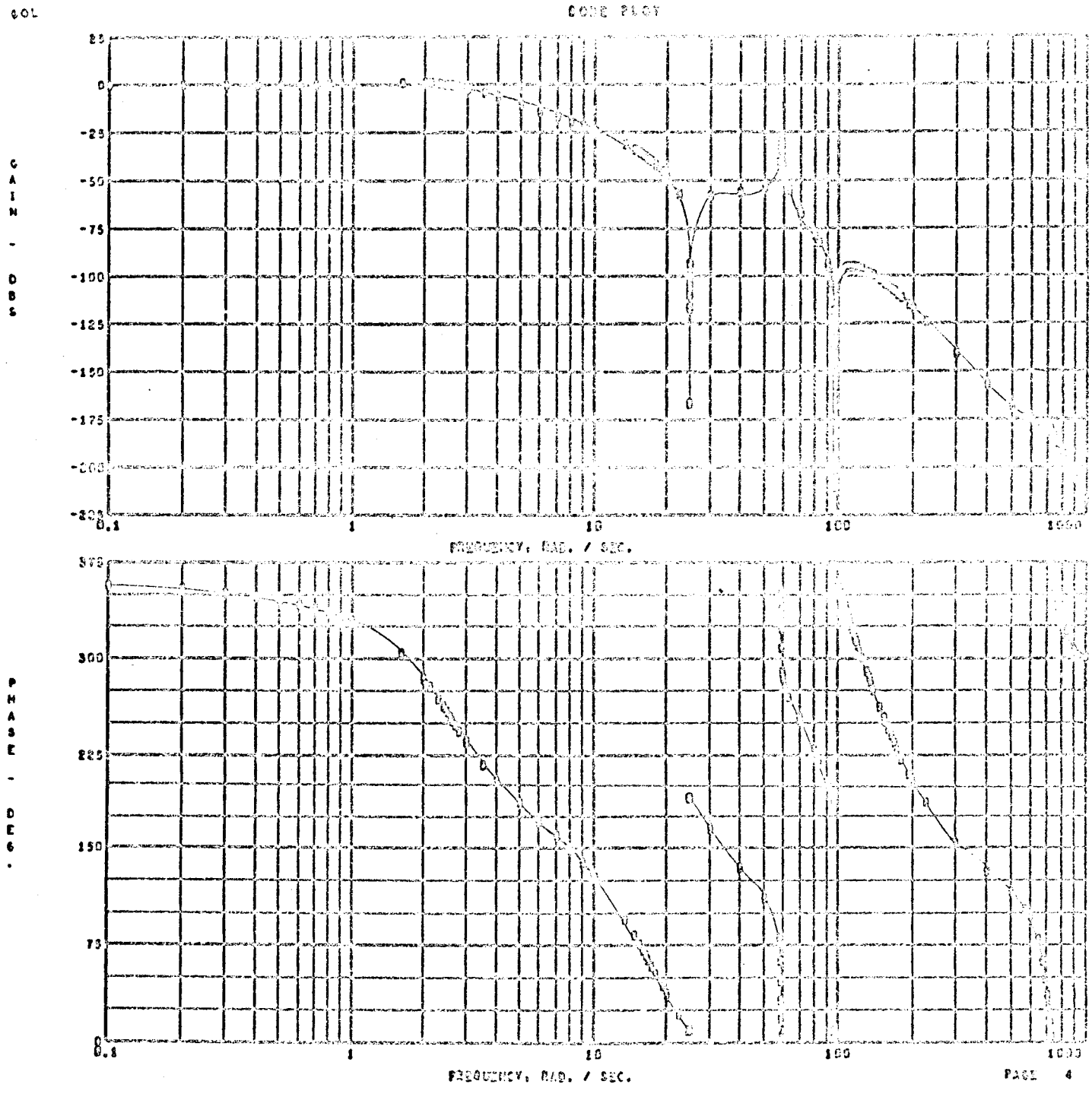

Frequency Response
Attitude Loop Closed
(ψ_F/ψ_C)

Figure 23